



OPEN ACCESS

EDITED BY

Vibhav Gautam,
Banaras Hindu University, India

REVIEWED BY

Santosh Kumar Singh,
Banaras Hindu University, India
Binbin Wei,
China Medical University, China

*CORRESPONDENCE

Xiang-Lan Piao,
xlpiao@muc.edu.cn

SPECIALTY SECTION

This article was submitted to
Ethnopharmacology,
a section of the journal
Frontiers in Pharmacology

RECEIVED 15 October 2022

ACCEPTED 21 November 2022

PUBLISHED 01 December 2022

CITATION

Qi Y-S, Xiao M-Y, Xie P, Xie J-B, Guo M,
Li F-F and Piao X-L (2022),
Comprehensive serum metabolomics
and network analysis to reveal the
mechanism of gypenosides in treating
lung cancer and enhancing the
pharmacological effects of cisplatin.
Front. Pharmacol. 13:1070948.
doi: 10.3389/fphar.2022.1070948

COPYRIGHT

© 2022 Qi, Xiao, Xie, Xie, Guo, Li and
Piao. This is an open-access article
distributed under the terms of the
[Creative Commons Attribution License
\(CC BY\)](https://creativecommons.org/licenses/by/4.0/). The use, distribution or
reproduction in other forums is
permitted, provided the original
author(s) and the copyright owner(s) are
credited and that the original
publication in this journal is cited, in
accordance with accepted academic
practice. No use, distribution or
reproduction is permitted which does
not comply with these terms.

Comprehensive serum metabolomics and network analysis to reveal the mechanism of gypenosides in treating lung cancer and enhancing the pharmacological effects of cisplatin

Yan-Shuang Qi, Man-Yu Xiao, Peng Xie, Jin-Bo Xie, Mei Guo, Fang-Fang Li and Xiang-Lan Piao*

School of Pharmacy, Minzu University of China, Beijing, China

Gypenosides (GYP) exerted anticancer activity against various cancers. However, the mechanism of GYP against lung cancer (LC) *in vivo* remains unclear. This study aims to reveal the potential mechanism of GYP against LC and enhancing cisplatin efficacy using a comprehensive analysis of metabolomics, network analysis. Pharmacodynamic results showed that GYP inhibited tumor growth, reduced tumor volume and tumor weight, and alleviated pathological symptoms in Lewis tumor-bearing mice, and GYP could enhance the anti-LC effects of cisplatin. Using serum metabolomics methods, 53 metabolites were found to be significantly altered in the model group, and the levels of 23 biomarkers were significantly restored after GYP treatment. GYP-related metabolic pathways involved six pathways, including alpha-linolenic acid metabolism, glutathione metabolism, sphingolipid metabolism, glycerophospholipid metabolism, tryptophan metabolism, and primary bile acid biosynthesis. 57 genes associated with differential metabolites of GYP recovery and 7 genes of 11 saponins of GYP against LC were screened by network analysis, the STRING database was used to find the association between 57 genes and 7 genes, and a compound-intersection gene-metabolite related gene-metabolite-pathway network was constructed, and STAT3, MAPK14, EGFR and TYMS might be the crucial targets of GYP against LC. Western blot results showed that GYP restored the levels of STA3, MAPK14, EGFR, and TYMS in the model group, and GYP also restored the levels of STAT3 and MAPK14 in the cisplatin group, indicating that

Abbreviations: GYP, Gypenosides; LC, Lung cancer; MTT, 3-(4,5-dimethylthiazol-2-yl)-2,5-diphenyltetrazolium bromide; OD, Optical density; LLC, Lewis lung carcinoma cell; RT, Retention time; SDS-PAGE, Sodium dodecyl sulfate polyacrylamide gel electrophoresis; EP, eppendorf; QC, Quality control; TICs, Total ion chromatograms; VIP, Variable important in projection; STAT3, Signal Transducer and Activator of Transcription 3; TYMS, Thymidylate synthase; MAPK14, Mitogen-activated protein kinase 14; EGFR, Epidermal Growth Factor Receptor.

GYP might exert anti-LC effects and enhance the pharmacological effects of cisplatin through MAPK14/STAT3 signaling pathway. Our method revealed the effect and mechanism of GYP on LC and the pharmacological effects of GYP-enhanced chemotherapeutic agent cisplatin, which provided some reference for the development of anti-cancer drugs.

KEYWORDS

Gynostemma pentaphyllum, gypenosides, cisplatin, metabolomics, lung cancer, network analysis

1 Introduction

Gynostemma pentaphyllum (Thunb.) Makino is an herbaceous vine of Cucurbitaceae (Kim et al., 2022a), *G. pentaphyllum* is widely used as herb or tea in Asia (Li et al., 2022). *G. pentaphyllum* contains flavonoids, saponins, polysaccharides and other substances. Gypenosides (GYP) is the main bioactive components in *G. pentaphyllum*, which has the effects of anti-oxidation, lowering blood lipid, lowering blood glucose and anti-cancer (Kim et al., 2022b). In Zhuang medicine (Liang and Zhong, 2005) and traditional Chinese medicine theory (Zhao et al., 2006), *G. pentaphyllum* was reported to be able to inhibit the growth of tumors. Lung cancer is the main cause of cancer-related death and one of the most common malignant tumors in the world (Li et al., 2021). Cisplatin is a platinum-based anticancer drug. It is the first-line drug for clinical chemotherapy of lung cancer, but cisplatin has side effects, cisplatin has been reported to be more effective in combination with traditional Chinese medicine than cisplatin alone (Qiu et al., 2021).

Metabolomics involves the systematic analysis of metabolites produced in cells, body fluids, tissues or organs under drug or pathological conditions (Schmidt et al., 2021). Generally, two techniques are used for metabolic analysis, namely, nuclear magnetic resonance (NMR) spectroscopy and mass spectrometry (Tayanloo-Beik et al., 2020). Metabolomics technology is now widely used to measure the response of endogenous metabolites to the whole body and find biomarkers of many cancers (Yang et al., 2020). Metabolomics plays a crucial role in biomarker discovery and mechanistic interpretation of lung cancer, providing a basis for biomarker screening, early diagnosis and staging of LC (Noreldeen et al., 2020). Metabolomics is a promising area in cancer research, which is divided into non-targeted and targeted metabolomics, and the purpose of non-targeted approaches is to obtain as many metabolites as possible from a range of biological samples (Cheung et al., 2019).

It is reported that GYP had anticancer effects on colorectal cancer, leukemia, oral cancer, hepatocellular carcinoma, bladder cancer, lung cancer and renal cell cancer (Ahmad et al., 2019), (Liu et al., 2021).

In our previous study, we explored the mechanism of GYP on A549 cells using network pharmacology and metabolomics (Qi et al., 2021). In this study, we established a Lewis lung cancer mouse model, and then used a combination of serum metabolomics and network analysis to discover GYP-related metabolite markers, and

clarified the anticancer mechanism of GYP and enhanced chemotherapeutic drugs pharmacological effects (Figure 1).

2 Materials and methods

2.1 Chemicals and reagents

Gypenosides (GYP) were provided by our own laboratory (Qi et al., 2021); Cisplatin was purchased from TargetMol (United States). β -actin (Zsgb-Bio, TA-09, 1:1000), STAT3 (Proteintech, 60199-1-Ig, 1:2000), TYMS (Proteintech, 15047-1-AP, 1:1000), MAPK14 (Proteintech, 66234-1-Ig, 1:2000), EGFR (Proteintech, 66455-1-Ig, 1:10000).

2.2 Animals and cell lines

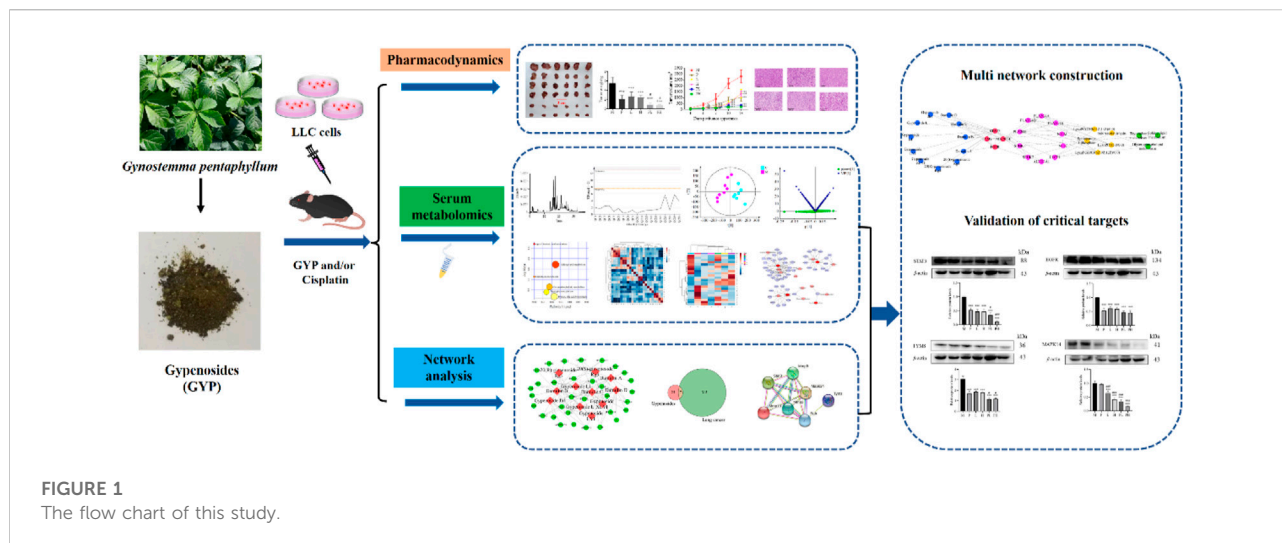
The Lewis lung carcinoma cell (LLC) line was bought from the National infrastructure of Cell Line Resource (Beijing, China) and cultured in DMEM medium (Gibco) in a humidified atmosphere (5% CO₂, 37°C). Pathogen free male C57BL/6N mice (18–20 g) were purchased from Beijing Vital River Laboratory Animal Technology Co., Ltd. (Beijing, China, approval number: SCXK-2016-0006).

2.3 Cell viability assay

Cell viability was evaluated by MTT assay. For each experiment, 1×10^4 cells were seeded in each well of 96 well plates. Then the cells were attached to the wall after 24 h and used with different concentrations of GYP (0, 120, 250, 500 μ g/ml) for 24 h. The OD values were detected at 490 nm using a microplate reader. There were 3 replicates in each group.

2.4 Mouse xenograft models and drug administration

The mice were housed in an animal room (24 \pm 2°C, 60 \pm 5% relative humidity) set to a 12 h dark/light cycle. Mice were fed water and standard laboratory food to adapt to the environment for 7 days



before the experiment. After one week, forty-two mice were used to build an LLC tumor-bearing mice model of LLC by subcutaneous injection with 0.1 ml LLC (2×10^7 /ml) cells. After the model was constructed successfully, mice were randomly divided into 7 groups, including control group [C], model group [M], cisplatin group [P] (cisplatin, 4 mg/kg), GYP low-dose group [L] (GYP, 40 mg/kg), GYP high-dose group [H] (GYP, 80 mg/kg), cisplatin + low-dose GYP group [PL] (cisplatin, 4 mg/kg; GYP, 40 mg/kg) and cisplatin + high-dose GYP group [PH] (cisplatin, 4 mg/kg; GYP, 80 mg/kg) ($n = 6$ each). GYP (dissolved in PBS, 8 mg/ml, 16 mg/ml) was intraperitoneally injected into the mice once a day at the dose of 0.1 ml/20 g (dose volume/body weight) for 14 days. Cisplatin (dissolved in PBS, 0.8 mg/ml) was intraperitoneally injected into the mice every other day at the dose of 0.1 ml/20 g (dose volume/body weight) for 7 days. The mice in the control group and model group were all given PBS at the equal volume. The body weights of mice were weighed and recorded every 2 days. The sarcoma sizes were measured and recorded every 3 days, and the length and width of the sarcoma were measured using a vernier caliper, tumor volume was calculated as follows: tumor size = tumor length \times (tumor width)²/2 (Wu et al., 2018). Mice were sacrificed on day 15 after successful tumor inoculation, and the blood were collected. Tumor tissues were further removed and weighed, half of which were fixed with 4% paraformaldehyde for HE staining, and the other half were snap-frozen with liquid nitrogen and placed in a -80°C freezer for future use.

2.5 Hematoxylin-eosin staining

The tumor tissues of each mouse were fixed in 4% paraformaldehyde and embedded in paraffin, and then tumor tissues were cut into 4 μm sections and stained with hematoxylin and eosin (HE).

2.6 Serum metabolomics analysis

2.6.1 Serum collection and preparation

The preparation and pretreatment of serum samples and QC samples were adjusted appropriately according to references (Cai et al., 2022). Mice were fasted in advance for 12 h, and blood was collected in 1.5 ml eppendorf (EP) tubes by retro-orbital bleeding after anesthesia, and then the blood was centrifuged (12000 r/min) for 20 min to collect serum samples. 10 μL of each sample was mixed to collect quality control (QC) samples. 100 μL serum samples were mixed with 400 μL acetonitrile to precipitate proteins, vortexed to pellet completely, and centrifuged at 12,000 r/min and 4°C for 20 min. 450 μL of the supernatant was drawn with a pipette and placed in a centrifugal concentrator for concentration and drying. 80% acetonitrile-water (v/v) was then added for reconstitution and vortexed for 2 min before UPLC-MS analysis.

2.6.2 UPLC-Q-TOF/MS condition

A Waters ACQUITY UPLC HSST3 column (1.8 μm , 2.1 \times 100 mm) was used for chromatographic separation, and the mobile phase consisted of 0.1% formic acid aqueous solution (phase A) and 0.1% formic acid acetonitrile (phase B) at a flow rate of 0.2 ml/min. Gradient elution conditions were properly adjust according to literature (Yao et al., 2022), as follows: 0–2 min, 99%–99% A; 2–3 min, 99%–65% A; 3–25 min, 60%–1% A; 25–30 min, 1% A; 30–30 min, 1%–99% A; 30–40 min, 99%–99% A. The total chromatographic run time was 40 min, the injection volume was 5 μL , and the column temperature was 35°C .

The mass spectrometer is a Q/TOF-MS system equipped with an electrospray ionization (ESI) source (Time of Flight™ 6600, AB SCIEX, United States). Nebulizer gas (GS 1), heater gas (GS 2) and Curtain gas was 40 psi, 40 psi, 35 psi, respectively; the

collision energy (CE), declustering potential (DP) and the collision energy spread (CES) were respectively 25/- 25 eV, 80/- 80 V and (\pm) 12.5 eV; The m/z scan range of TOF MS and IDA MS/MS was 100–1500 and 50-1000, respectively. The ion source temperature was 450°C. After LC- (\pm) ESI-MS in two ion modes was collected, MSConvert software was used to convert Wiff format files to mzXML format files, then XCMS software is used to obtain a two-dimensional data array including mass to charge ratio (m/z), retention time (RT) and peak area.

2.6.3 Multivariate statistical analysis

The data matrices of two ion modes were imported into SIMCA software (Swedish Umetrics version 14.0) for unsupervised principal component analysis (PCA), validation plot analysis, supervised orthogonal partial least squares discriminant analysis (OPLS-DA) and VIP + S plot analysis, respectively. All QC samples were subjected to Hotelling's T² region to test the stability of the instrument. Variable importance in prediction (VIP) > 1.0, combined with an absolute value of *p*corr greater than 0.5 as well as the *p*-value of *t*-test < 0.05, was used to seek differential metabolites between the control group [C] and the model group [M]. The relative contents of differential metabolites between the 7 groups were compared to seek GYP-related differential metabolites.

2.6.4 Determination of potential biomarker, metabolic pathway analysis, correlation analysis and heatmap analysis

HMDB database (<https://hmdb.ca/>) and METLIN database (<https://metlin.scripps.edu/>) were used to identify the differential metabolites between the control group and model group, and then the relative contents of different metabolites in 7 groups were compared by GraphPad Prism 9 software for exploring the biological effect of GYP on lung cancer, then the 23 metabolites recalled by GYP were imported into MetaboAnalyst 5.0 database (<https://www.metaboanalyst.ca/>) for analysing metabolic pathway, pearson correlation analysis and heatmap analysis.

2.7 Screening for the intersection of compounds targets and disease targets

We obtained GYP-related targets from SwissTargetPrediction database (<http://swisstargetprediction.ch/>). To deeply dissect the anti-LC effects of GYP on LLC mice, lung cancer associated genes were obtained from National Center for Biotechnology Information database (<https://www.ncbi.nlm.nih.gov/>) and OMIM database (<https://omim.org/>). Then the intersection genes of compounds targets and disease targets were exported into STRING database (<https://cn.string-db.org/>) and Cytoscape_v 3.9.0 software for Protein-Protein Interaction (PPI) network construction.

2.8 Multi network construction

In order to investigate how GYP exerts its anti-lung cancer effects by regulating metabolites and metabolic pathways as well as enhancing the anti-lung cancer effects of chemotherapeutic agents, a compound-intersection genes-metabolite related gene-metabolite-pathway network was constructed.

2.9 Western blot analysis

Total protein was extracted from tumor tissues, total protein concentration was determined with a BCA kit (Beyotime), then SDS-PAGE electrophoresis was used to separate the same amounts of samples, then the protein was transferred to PVDF membrane, and then the primary antibody (β -actin, STAT3, TYMS, MAPK14, EGFR) and secondary antibody were incubated for 2 h respectively, then the PVDF membranes were detected by ECL (Beyotime). The bands were quantitatively analyzed by ImageJ software.

2.10 Statistical analysis

All experiments were reported as mean \pm SD. One-way analysis of variance (ANOVA) was used for comparing differences among the control group [C], model group [M], cisplatin group [P], GYP low-dose group [L], GYP high-dose group [H], cisplatin + low-dose GYP group [PL], cisplatin + high-dose GYP group [PH]. A *p*-value < 0.05 was considered statistically significant.

3 Results

3.1 GYP inhibited the viability of LLC cells

According to Figure 2A, the cell viability was 97.55%, 45.21%, and 15.32% after treated with 125, 250, and 500 μ g/ml GYP, respectively. GYP could suppress the proliferation of LLC cells in a dose-dependent manner, and GYP had no significant effect on the activity of BEAS-2B cells within the maximum dose of 500 μ g/ml of GYP administered. The IC₅₀ value of GYP on LLC cells was 272.5 μ g/ml.

3.2 GYP decreased the tumor volume and tumor weight of the model group and cisplatin group

The anti-cancer effect of GYP *in vivo* was then conducted on Lewis tumor-bearing mice (Figures 2B–E). Compared with M group, the tumor volume of other 5 groups (P, L, H, PL and PH group) significantly decreased, of which PL group and PH group

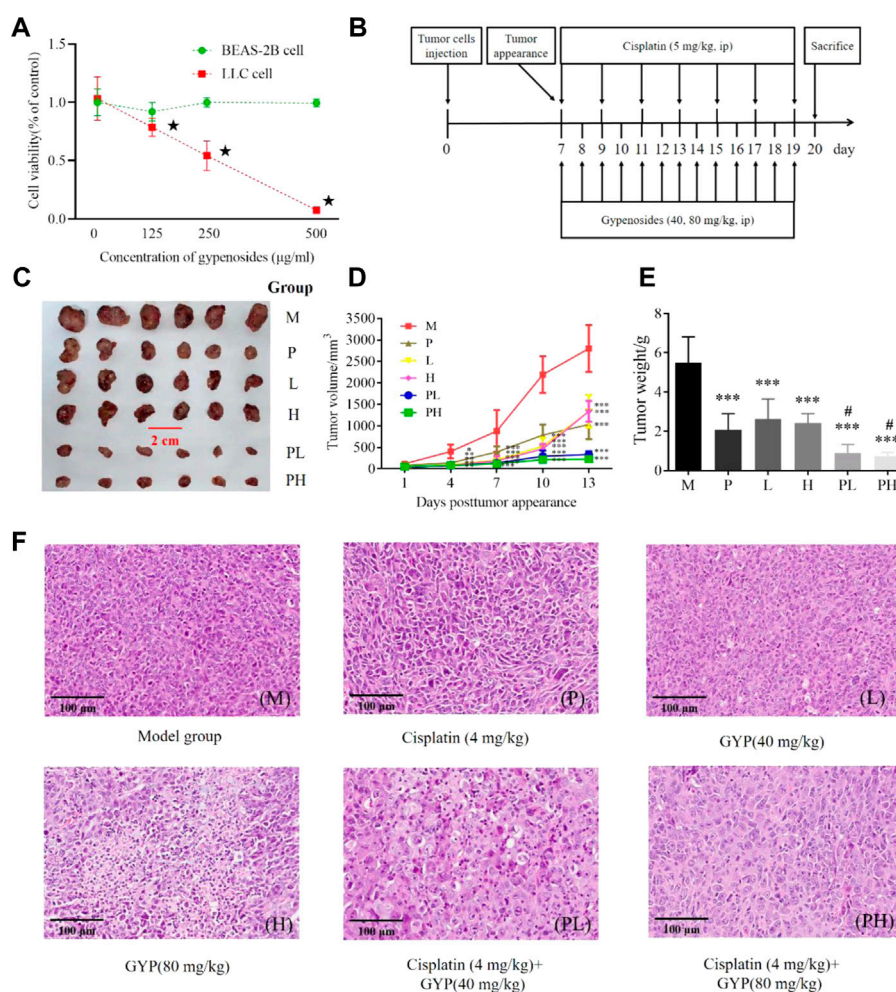


FIGURE 2

GYP suppressed the growth of xenografted LLC tumors and enhanced cisplatin efficacy in C57BL/6 mice. The cell viability of GYP against LLC cells and BEAS-2B cells, vs. 0 mg/ml GYP, * $p < 0.001$ (A); Administration procedures in animal experiment (B); Tumor visualization of 6 groups (C); The tumor volumes (D) and tumor weights (E) of 6 tumor-bearing group (M: model group, P: cisplatin group, L: low-dose GYP group, H: high-dose GYP group, PL: cisplatin + low-dose GYP group, PH: cisplatin + high-dose GYP group; vs. Control group, * $p < 0.05$, ** $p < 0.01$, *** $p < 0.001$; vs. Model group, # $p < 0.05$); The histopathology sections (H&E, magnification = ×40, 50 µm) of tumor of 6 groups (F).

decreased more (Figure 2C). Compared with M group, the tumor weight of P group, L group, H group, PL group and PH group significantly decreased, of which PL group and PH group decreased more (Figures 2D,E). Thus, GYP could suppress sarcoma growth and enhance the antitumor efficacy of cisplatin.

Histopathological analysis of tumor tissue suggested that the tumor cells in the model [M] group were closely arranged, with obvious nucleoli and diffuse distribution. In the cisplatin + GYP groups (PL and PH group), compared with the single GYP treatment groups (L and H group) and the single cisplatin treatment group (P group), the area with unclear boundary and nuclear disappearance is larger, indicating that GYP had anticancer effect and could enhance the pharmacological effects of cisplatin (Figure 2F).

3.3 Metabolomic analysis

The total ion chromatograms (TICs) (Figure 3) were obtained from QC, control [C], model [M], cisplatin [P], GYP low-dose [L], GYP high-dose [H], cisplatin + low-dose GYP [PL], cisplatin + high-dose GYP [PH] group using UPLC-Q-TOF/MS conditions. Endogenous metabolites with molecular weight less than 1000 Da could be well separated within 40 min. A total 27807 and 27665 ions were respectively extracted from the positive and negative datasets.

The PCA score plots (Figures 4A,B) of 7 groups in two modes showed that GYP treatment had effect on the metabolic profile of LLC mice. According to Figures 5A,F, the Hotelling's T² range map showed that there were no

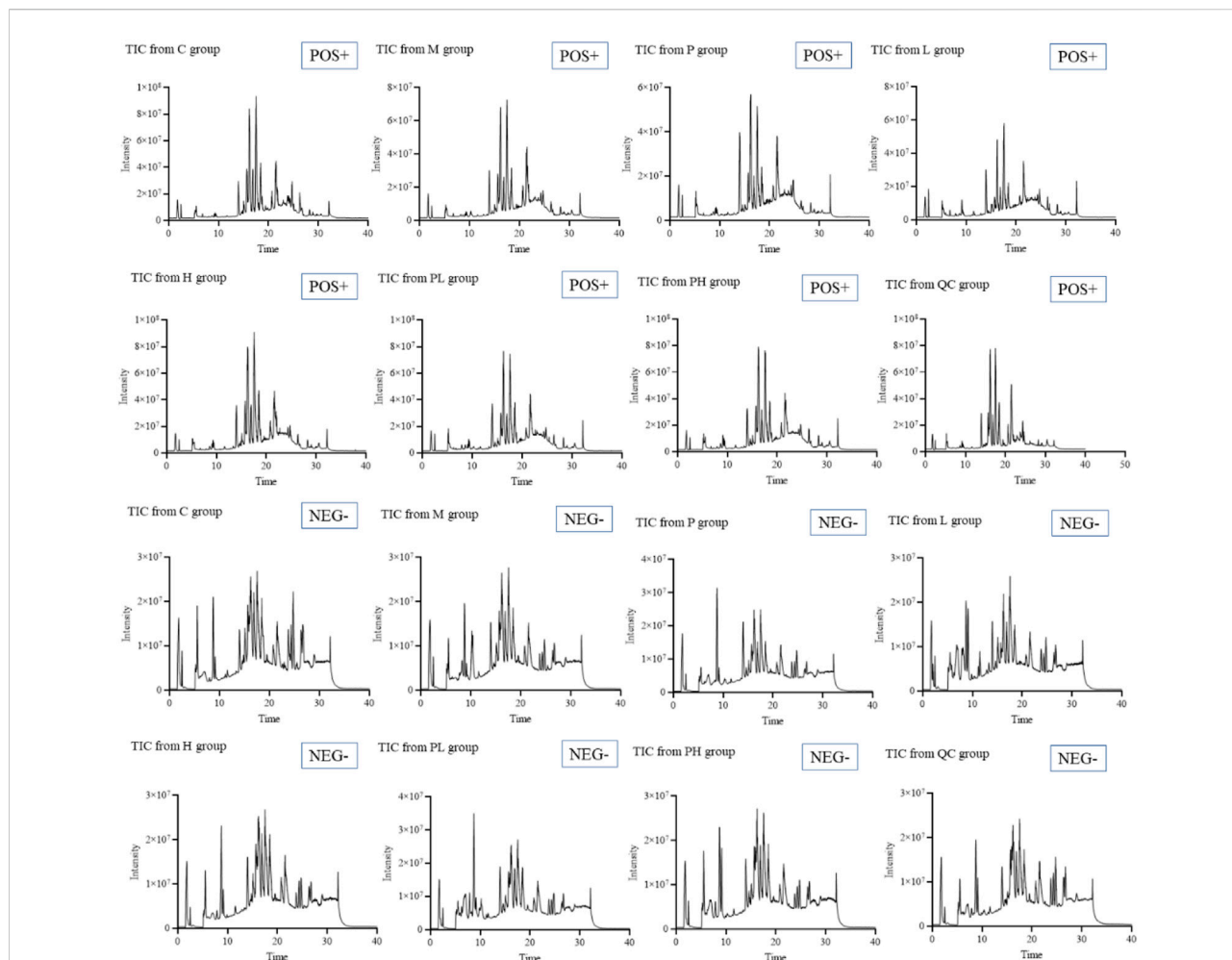


FIGURE 3 Total ions chromatograms (TICs) of control [C], model [M], cisplatin [P], GYP low-dose [L], GYP high-dose [H], cisplatin + low-dose GYP [PL] and cisplatin + high-dose GYP [pH] in the positive model (POS +) and negative model (NEG -).

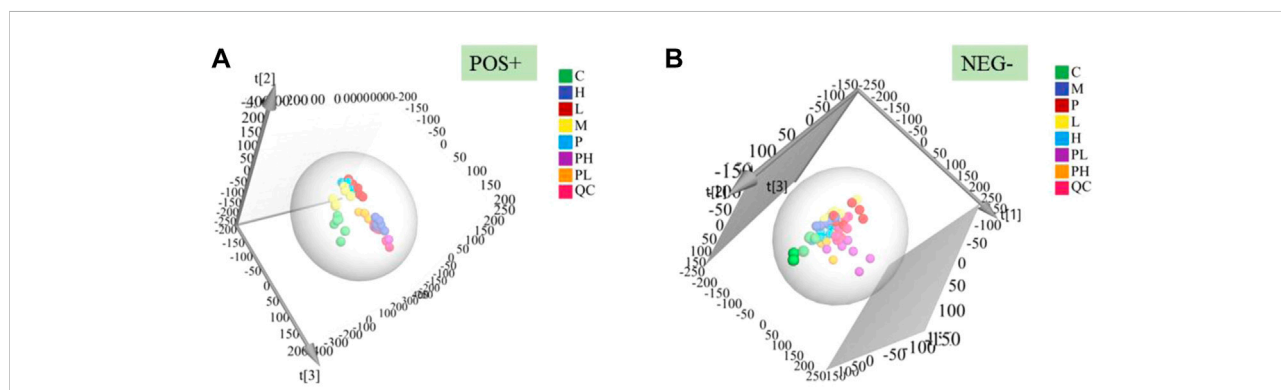


FIGURE 4 PCA score plots in positive (A) and negative (B) ion mode of serum samples among control [C], model [M], cisplatin [P], GYP low-dose [L], GYP high-dose [H], cisplatin + low-dose GYP [PL], cisplatin + high-dose GYP [pH] group and QC group [QC].

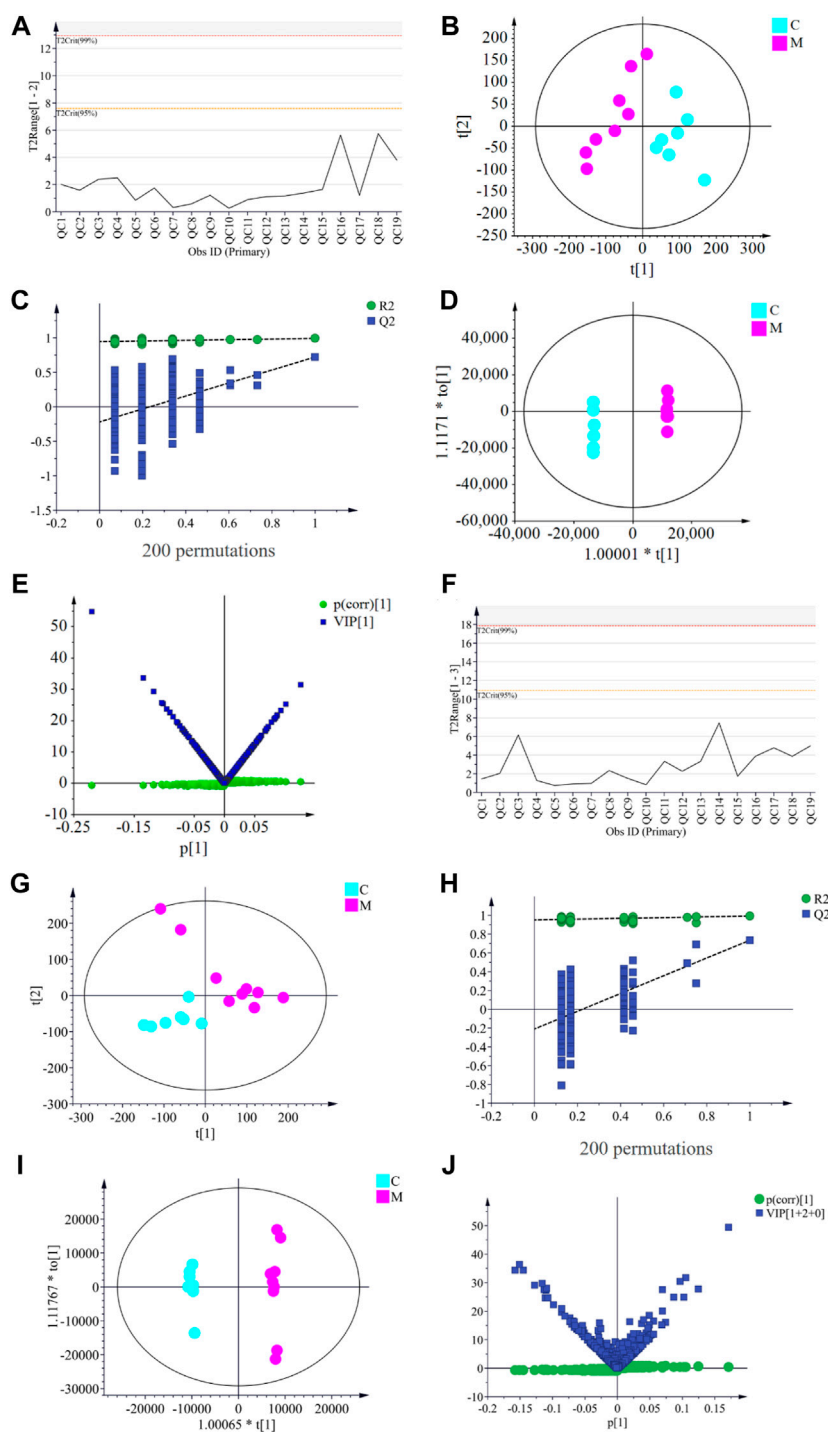


FIGURE 5 Hotelling's T2 plots of QC group (A and F); PCA (B and G), validation plot (C and H), OPLS-DA (D and I), VIP + S plots (E and J) of serum samples between control [C] group and model [M] group in positive model (A–E) and negative model (F–J).

serious outliers in all samples in the QC group, indicating the reliability and accuracy of the analysis. The PCA score plots (Figures 5B,G) and OPLS-DA score plots (Figures 5C,H)

demonstrated that the C group and M group were well separated, which proved that the Lewis lung cancer mouse model is successful. The OPLS-DA model validation plots

TABLE 1 Identified differential metabolites in serum between control group [C] and model group [M] in positive ion model and negative ion model.

Name	Molecular formula	Mode	RT/min	ppm	VIP	p _{corr} -value	p-value
Aminopropylcadaverine	C ₈ H ₂₁ N ₃	M + H	1.60	-1.87	1.15	0.71	<0.001
Choline	C ₅ H ₁₄ NO	M + H	1.88	-1.92	2.11	-0.60	0.0010
Taurine	C ₂ H ₇ NO ₃ S	M - H	1.95	0.81	1.04	-0.79	0.0155
Formiminoglutamic acid	C ₆ H ₁₀ N ₂ O ₄	M + H	2.39	-2.28	1.29	-0.92	<0.001
Cytosine	C ₄ H ₅ N ₃ O	M + H	2.47	-2.68	1.20	-0.81	<0.001
Cytidine	C ₉ H ₁₃ N ₃ O ₅	M + H	2.47	0.41	1.18	-0.74	<0.001
Indole-3-acetamide	C ₁₀ H ₁₀ N ₂ O	M + H	2.48	-4.57	1.24	-0.90	<0.001
Pseudouridine	C ₉ H ₁₂ N ₂ O ₆	M - H	2.50	2.89	2.37	0.77	0.0026
4-(2-Aminophenyl)-2,4-dioxobutanoic acid	C ₁₀ H ₉ NO ₄	M - H	5.40	1.46	1.12	-0.60	0.0108
N-Acetyl-L-methionine	C ₇ H ₁₃ NO ₃ S	M - H	5.43	-4.21	1.81	-0.93	<0.001
Undecanedioic acid	C ₁₁ H ₂₀ O ₄	M - H	5.66	1.39	1.24	-0.69	<0.001
Butenylcarnitine	C ₁₁ H ₁₉ NO ₄	M - H	6.01	1.32	1.66	-0.68	<0.001
Indoleacetaldehyde	C ₁₀ H ₉ NO	M - H	6.25	0.63	1.05	0.72	<0.001
Tetradecanedioic acid	C ₁₄ H ₂₆ O ₄	M - H	7.33	0.78	5.65	-0.68	<0.001
3, 5-Tetradecadiencarnitine	C ₂₁ H ₃₇ NO ₄	M + H	10.51	-1.08	1.09	-0.66	<0.001
Dodecanoylcarnitine	C ₁₉ H ₃₈ NO ₄	M + H	10.65	-0.87	1.13	-0.65	0.0020
Pimelylcarnitine	C ₁₄ H ₂₅ NO ₆	M + H	12.02	-1.32	1.09	-0.73	0.0110
Sphingosine	C ₁₈ H ₃₇ NO ₂	M + H	12.50	-1.00	1.88	-0.66	<0.001
3-Oxododecanoic acid	C ₁₂ H ₂₂ O ₃	M - H	12.61	2.35	2.52	-0.58	<0.001
10,11-dihydro-20-trihydroxy-leukotriene B4	C ₂₀ H ₃₄ O ₇	M - H	13.34	2.60	9.06	-0.60	<0.001
Sphingosine 1-phosphate	C ₁₈ H ₃₈ NO ₅ P	M + H	13.74	-0.79	2.45	0.72	<0.001
Dopamine 4-sulfate	C ₈ H ₁₁ NO ₅ S	M + Na	14.07	4.30	2.88	-0.62	<0.001
12-Hydroxydodecanoic acid	C ₁₂ H ₂₄ O ₃	M - H	14.32	1.86	2.16	-0.65	<0.001
Sphinganine 1-phosphate	C ₁₈ H ₄₀ NO ₅ P	M + H	14.41	-2.09	1.38	0.68	<0.001
LysoPA (8:0/0:0)	C ₁₁ H ₂₃ O ₇ P	M + H	14.61	2.67	1.01	-0.60	0.0018
LysoPC(18:3 (6Z,9Z,12Z)/0:0)	C ₂₆ H ₄₈ NO ₇ P	M + H	14.80	1.35	12.14	-0.69	<0.001
12S-HHT	C ₁₇ H ₂₈ O ₃	M - H	15.07	1.07	3.26	-0.77	<0.001
LysoPE (18:0/0:0)	C ₂₃ H ₄₈ NO ₇ P	M + H	15.16	-1.04	6.65	-0.77	0.0176
VPGR Enterostatin	C ₂₃ H ₄₀ N ₈ O ₆	M + Na	15.66	4.36	4.23	-0.66	<0.001
LysoPC(15:0/0:0)	C ₂₃ H ₄₈ NO ₇ P	M + H	15.79	0.21	6.65	-0.74	0.0160
Taurodeoxycholic acid	C ₂₆ H ₄₅ NO ₆ S	M - H	15.95	0.60	2.31	0.51	<0.001
LysoPC(20:0/0:0)	C ₂₈ H ₅₈ NO ₇ P	M + H	17.33	-1.63	4.52	-0.63	<0.001
Stearoylcarnitine	C ₂₅ H ₄₉ NO ₄	M + H	17.34	-0.93	5.02	0.93	<0.001
LysoPC(20:3 (8Z,11Z,14Z)/0:0)	C ₂₈ H ₅₂ NO ₇ P	M - H	17.63	2.39	2.69	-0.72	<0.001
LysoPC(22:6 (4Z,7Z,10Z,13Z,16Z,19Z)/0:0)	C ₃₀ H ₅₀ NO ₇ P	M + H	17.75	-4.75	1.07	0.59	<0.001
LysoPE (P-16:0/0:0)	C ₂₁ H ₄₄ NO ₆ P	M - H	18.26	0.69	2.36	-0.70	<0.001
PI(18:0/18:0)	C ₄₅ H ₈₇ O ₁₃ P	M - H	18.44	2.20	3.93	-0.65	<0.001
LysoPE (20:2 (11Z,14Z)/0:0)	C ₂₅ H ₄₈ NO ₇ P	M - H	19.05	1.19	2.57	0.80	<0.001
LysoPC(20:2 (11Z,14Z)/0:0)	C ₂₈ H ₅₄ NO ₇ P	M + H	19.40	-1.46	3.98	0.70	<0.001
LysoPC(P-18:0/0:0)	C ₂₆ H ₅₄ NO ₆ P	M + H	19.49	-0.39	8.12	-0.78	<0.001
LysoPE (0:0/22:1 (13Z))	C ₂₇ H ₅₄ NO ₇ P	M + H	20.20	-1.49	3.11	0.53	0.0037
Stearidonic acid	C ₁₈ H ₂₈ O ₂	M - H	21.36	2.18	4.69	-0.85	<0.001
Oleamide	C ₁₈ H ₃₅ NO	M + H	22.60	-1.06	1.31	-0.52	0.0034
2-Hexaprenyl-3-methyl-5-hydroxy-6-methoxy-1,4-benzoquinol	C ₃₈ H ₅₈ O ₄	M - H	22.94				<0.001
Tetradecanoylcarnitine	C ₂₁ H ₄₂ NO ₄	M + H	23.10	-1.07	3.74	0.66	<0.001
Oleoylethanolamide	C ₂₀ H ₃₉ NO ₂	M + H	23.26	-1.84	1.09	-0.56	0.0207
Guanosine triphosphate adenosine	C ₂₀ H ₂₇ N ₁₀ O ₁₇ P ₃	M + Na	25.79	2.39	3.12	0.78	<0.001
MG (14:0/0:0/0:0)	C ₁₇ H ₃₄ O ₄	M - H	26.38	1.00	2.66	-0.77	<0.001

(Continued on following page)

TABLE 1 (Continued) Identified differential metabolites in serum between control group [C] and model group [M] in positive ion model and negative ion model.

Name	Molecular formula	Mode	RT/min	ppm	VIP	<i>p</i> corr-value	<i>p</i> -value
LysoPC(6:0/0:0)	C ₁₄ H ₃₀ NO ₇ P	M - H	26.38	-4.24	1.01	-0.69	<0.001
Cholesterol sulfate	C ₂₇ H ₄₆ O ₄ S	M - H	26.72	0.64	3.51	-0.65	<0.001
Androsterone sulfate	C ₁₉ H ₃₀ O ₅ S	M - H	27.66	4.33	5.00	-0.75	<0.001
13'-Hydroxy-alpha-tocopherol	C ₂₉ H ₅₀ O ₃	M + Na	28.09	-1.92	4.18	-0.62	<0.001
12,13-DHOME	C ₁₈ H ₃₄ O ₄	M + Na	31.88	-2.97	1.03	0.62	<0.001

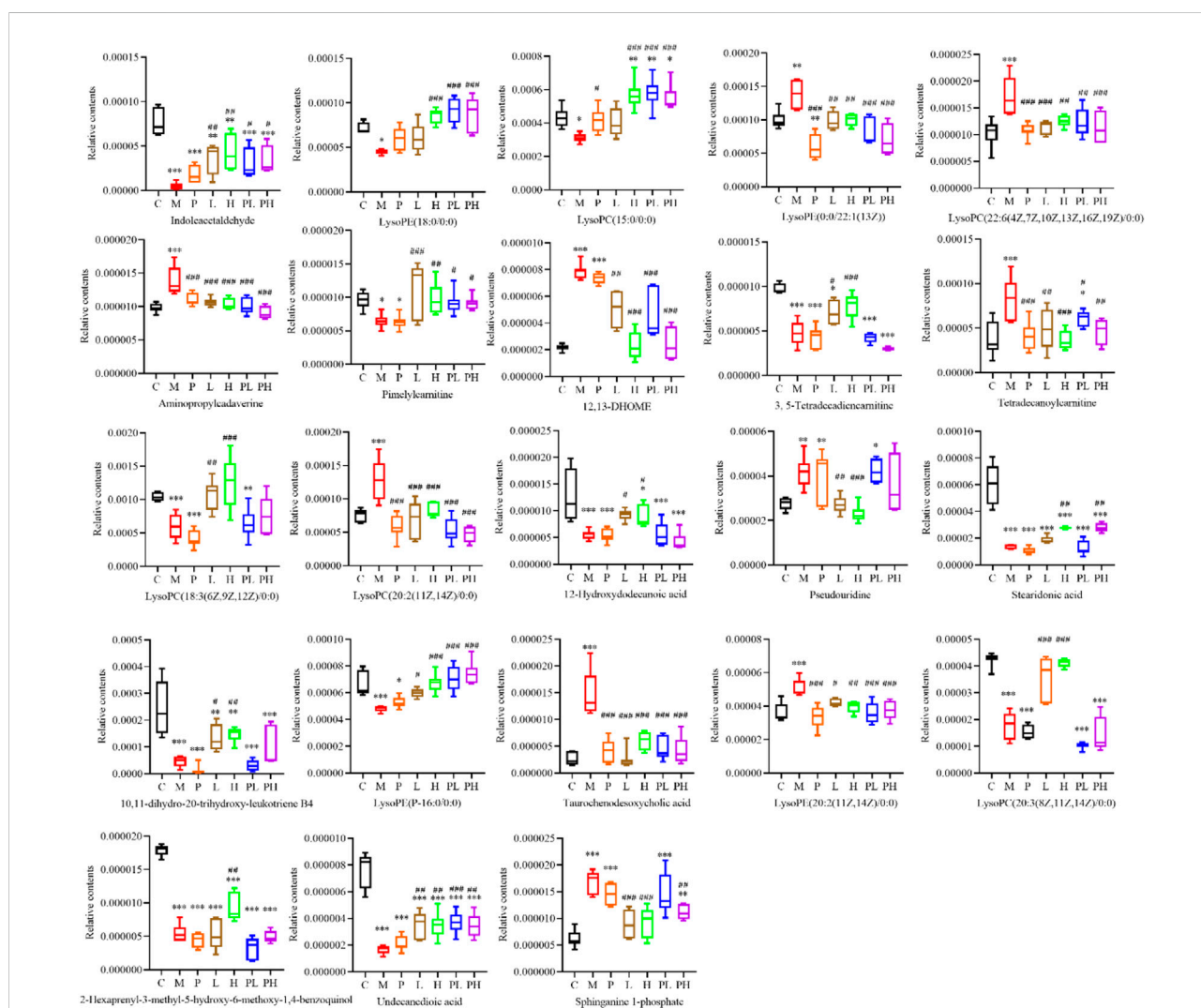


FIGURE 6 GYP significantly recovered the levels of 23 differential metabolites. Data were analyzed by One-way ANOVA analysis and represented as means ± SD (n = 6). (C: control group, M: model group, P: cisplatin group, L: low-dose GYP group, H: high-dose GYP group, PL: cisplatin + low-dose GYP group, PH: cisplatin + high-dose GYP group; vs. Control group, **p* < 0.05, ***p* < 0.01, ****p* < 0.001; vs. Model group, #*p* < 0.05, ##*p* < 0.01, ###*p* < 0.001).

showed that R2 and Q2 values of all points on the left were less than those of the rightmost point, which proves that the model was successful (Figures 5D,I). Then VIP + S-plot scatter plots (Figures 5E,J) were used to seek the differential metabolites between the C group and the M group, then 53 differential biomarkers (Table 1) of LLC mice were identified by HMDB database, METLIN database and Analyst[®]TF 1.6 Software in positive and negative datasets.

The relative contents of 53 differential metabolites among 7 groups (including control [C], model [M], cisplatin [P], GYP low-dose [L], GYP high-dose [H], cisplatin + low-dose GYP [PL] and cisplatin + high-dose GYP [pH]) was compared by GraphPad Prim 9 software (Supplementary Figure S1). As shown in Figure 6, GYP could regulate the metabolic disorder caused by LLC, a total of 23 metabolites had a tendency to recover to the C group level, in other words, a total of 23 potential metabolites in GYP low-dose [L] and GYP high-dose [H] group could be recalled to the content close to the C group compared with M group, including indoleacetaldehyde, LysoPE (18:0/0:0), LysoPC(15:0/0:0), LysoPE (0:0/22:1 (13Z)), LysoPC(22:6 (4Z,7Z,10Z,13Z,16Z,19Z)/0:0), aminopropylcadaverine, pimelylcarnitine, 12,13-DHOME, 3,5-Tetradecadienecarnitine, tetradecanoylcarnitine, LysoPC(18:3 (6Z,9Z,12Z)/0:0), LysoPC(20:2 (11Z,14Z)/0:0), 12-Hydroxydodecanoic acid, pseudouridine, stearidonic acid, 10,11-dihydro-20-trihydroxy-leukotriene B4, LysoPE (P-16:0/0:0), taurochenodesoxycholic acid, LysoPE (20:2 (11Z,14Z)/0:0), LysoPC(20:3 (8Z,11Z,14Z)/0:0), 2-Hexaprenyl-3-methyl-5-hydroxy-6-methoxy-1,4-benzoquinol, Undecanedioic acid, sphinganine 1-phosphate.

3.4 Metabolic pathway analysis of 23 metabolites associated with GYP treatment

For exploring the effect of GYP on Lewis tumor-bearing mice, 23 metabolites of GYP on LLC mice were introduced into MetaboAnalyst 5.0 database to select *Mus musculus* (KEGG) for path Library for metabolic pathway analysis. According to Figure 7A, we could judge that the effect of GYP on Lewis tumor-bearing mice may be related to six metabolic pathways, including alpha-Linolenic acid metabolism, glutathione metabolism, sphingolipid metabolism, glycerophospholipid metabolism, tryptophan metabolism, primary bile acid biosynthesis. The metabolite involved in alpha-Linolenic acid metabolism was stearidonic acid; The metabolite related to sphingolipid metabolism was sphinganine 1-phosphate; Aminopropylcadaverine was related to glutathione metabolism; The metabolites involved in glycerophospholipid metabolism was LysoPC(15:0/0:0), LysoPC(22:6 (4Z,7Z,10Z,13Z,16Z,19Z)/0:0), LysoPC(18:3 (6Z,9Z,12Z)/0:0), LysoPC(20:2 (11Z,14Z)/

0:0); Indoleacetaldehyde was involved in tryptophan metabolism; The metabolite related to primary bile acid biosynthesis was taurochenodesoxycholic acid.

3.5 Pearson correlation analysis and heatmap analysis

Pearson correlation analysis (Figure 7B) was used to study the correlation between 23 different metabolites, in which there was a strong positive correlation between undecanedioic acid and 10,11-dihydro-20-trihydroxy-leukotriene B4, stearidonic acid and Hexaprenyl-3-methyl-5-hydroxy-6-methoxy-1,4-benzoquinol, LysoPE (18:0/0:0) and LysoPC(15:0/0:0). There was a strong negative correlation between these metabolites, such as 3, 5-Tetradecadienecarnitine and LysoPC(20:2 (11Z,14Z)/0:0), pseudouridine and LysoPE (20:2 (11Z,14Z)/0:0). These results suggest that these differential metabolites were interrelated. The heatmap analysis (Figure 7C) was used to analyze the relative content of 23 metabolites in 7 groups.

3.6 Construction of a metabolite-target network

The KEGG ID of metabolites of GYP on lung cancer was introduced into MetScape (a plug-in of Cytoscape) to build the metabolite-target network (Figure 8). The related genes of LysoPC(15:0/0:0), LysoPC(22:6 (4Z,7Z,10Z,13Z,16Z,19Z)/0:0), LysoPC(18:3 (6Z,9Z,12Z)/0:0), LysoPC(20:2 (11Z,14Z)/0:0) were respectively LYPLA1, LYPLA2, CLC, PLA2G4E, CLCF1, LYPLA3, PLA2G4F, PLA2G2D, PLA2G4D, LGALS13, PLA2G2E, LCAT, PLA2G3, PLA2G1B, PLA2G2A, PLA2G4A, PLA2G5, PLA2G2F, PLA2G12A, PLA2G6, PLA2G10, PLA2G12B, PLA2G4C, LOC100137047-PLA2G4B; Sphinganine 1-phosphate related genes included CHMP4A, NT5C, SPHK2, NT5M, DUSP11, PPAP2A, PPAP2C, PPAP2B, SPHK1, SGPL1; Indoleacetaldehyde related genes included ALDH2, ALDH3A1, ALDH1B1, ALDH1A3, ALDH9A1, ALDH3A2, ABP1, AOC2, MAOA, MAOB, ALDH7A1, AOC3; Taurochenodeoxycholate related gene was BAAT. A total of 57 metabolite-related genes were obtained for the subsequent analysis.

3.7 Network analysis

In our previous report, 11 saponin components in GYP were identified by HPLC-MS-IT-TOF Network pharmacology analysis (Qi et al., 2021). Then the compound-target network between 11 saponins and their related genes was constructed (Figure 9A), this network includes 11 components and 32 target genes. 32 GYP related genes were retrieved from

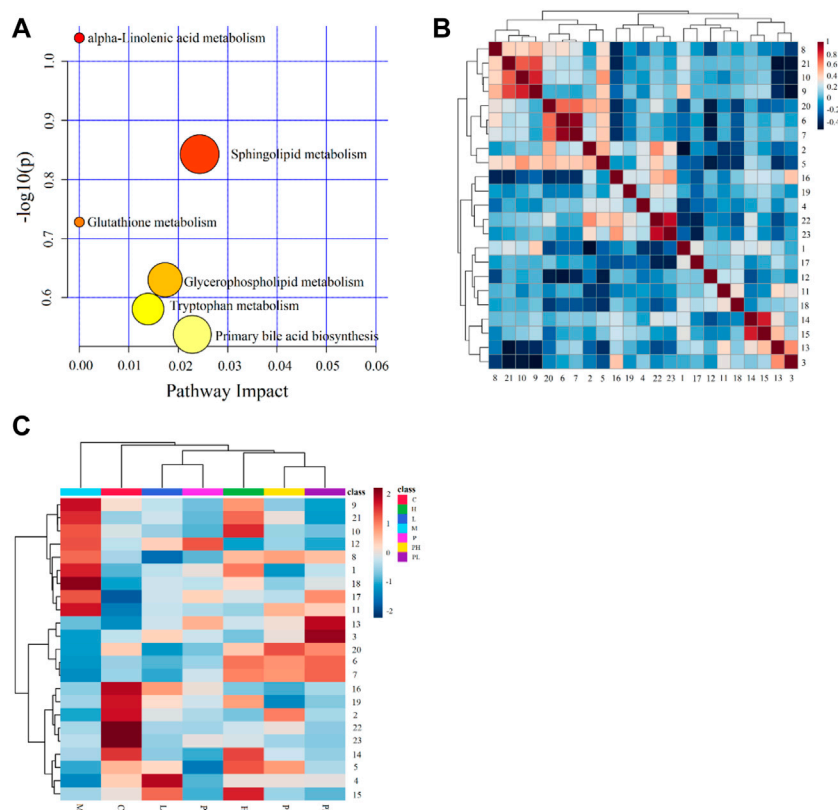


FIGURE 7

Pathway analysis of 23 differential metabolites of GYP on LLC mice (**A**); Pearson correlation analysis results of 23 differential metabolites, red indicates positive correlation and blue indicates negative correlation (**B**); Heatmap analysis of 23 differential metabolites among 7 groups (**C**). (Metabolites 1–23 represent Aminopropylcadaverine, Indoleacetaldehyde, 3,5-Tetradecadiencarnitine, Pimelylcarnitine, LysoPC [18:3 (6Z,9Z,12Z)/0:0], LysoPE (18:0/0:0), LysoPC (15:0/0:0), LysoPC [22:6 (4Z,7Z,10Z,13Z,16Z,19Z)/0:0], LysoPC [20:2 (11Z,14Z)/0:0], LysoPE [0:0/22:1 (13Z)], Tetradecanoylcarnitine, 12,13-DHOME, Pseudouridine, Undecanedioic acid, 10,11-dihydro-20-trihydroxy-leukotriene B4, 12-Hydroxydodecanoic acid, Sphinganine 1-phosphate, Taurochenodesoxycholic acid, LysoPC [20:3 (8Z,11Z,14Z)/0:0], LysoPE (P-16:0/0:0), LysoPE [20:2 (11Z,14Z)/0:0], Stearidonic acid, 2-Hexaprenyl-3-methyl-5-hydroxy-6-methoxy-1,4-benzoquinol).

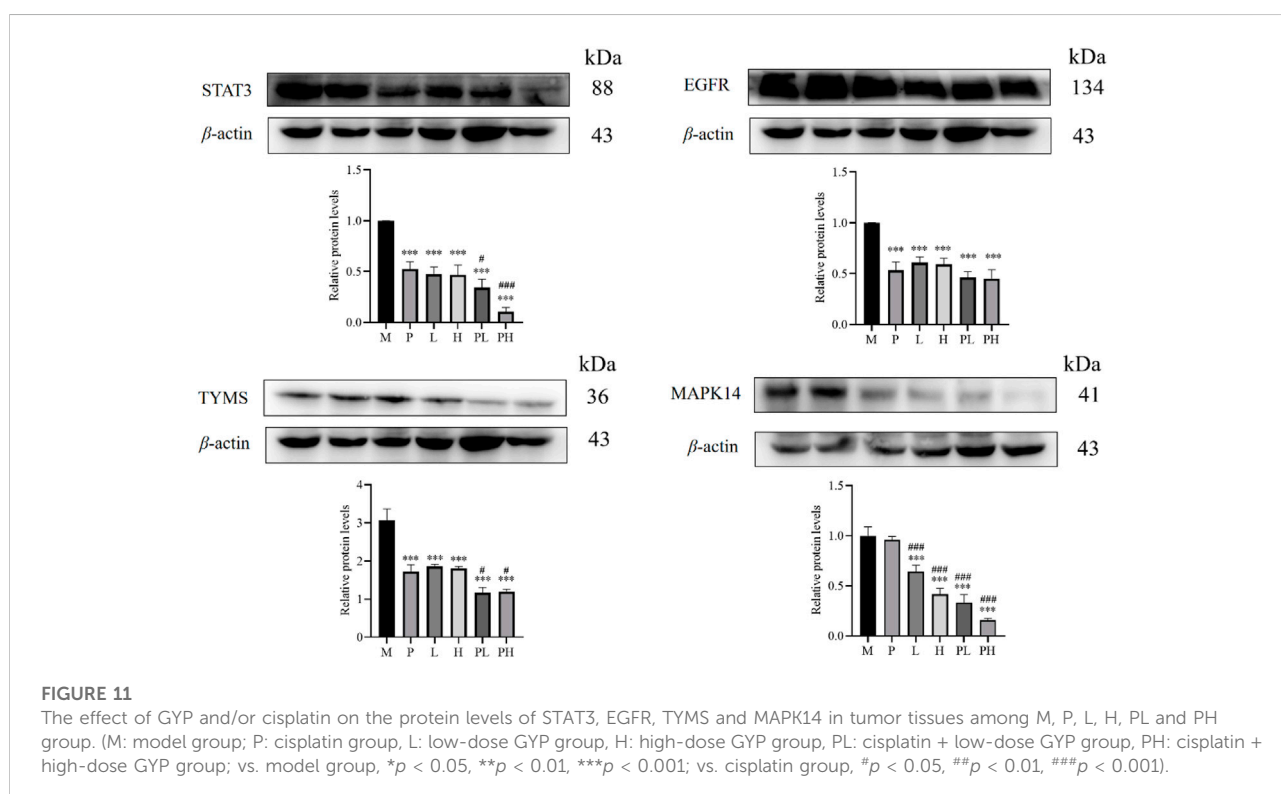
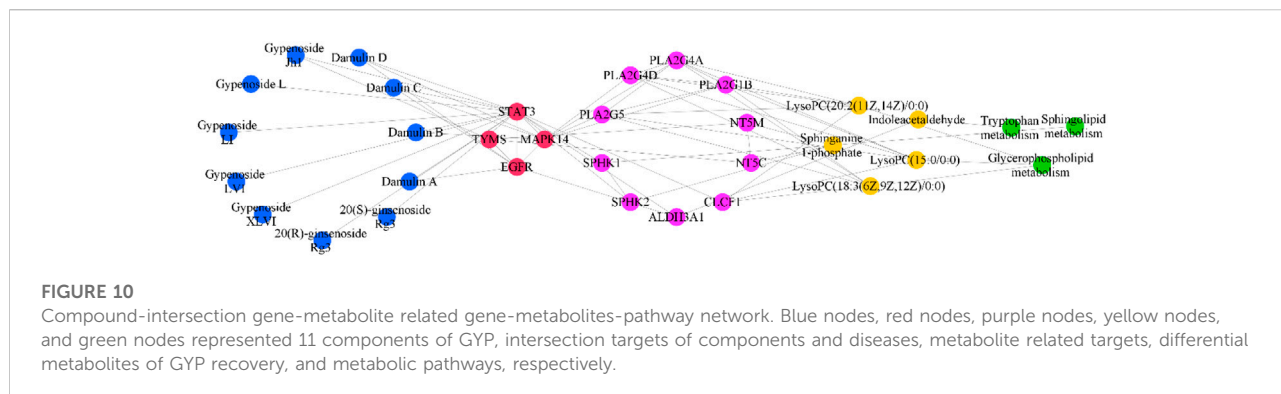
SwissTargetPrediction database, 322 LC related targets were retrieved from NCBI-gene database (<https://www.ncbi.nlm.nih.gov/gene>). There are 7 intersection genes of 11 components and diseases, namely STAT3, MMP9, MMP2, MMP13, EGFR, TYMS, MAPK14 (Figures 9B,C).

3.8 Multi network construction

The compound-intersection genes-metabolite related gene-metabolite-pathway network (Figure 10) showed that 11 saponins of GYP might indirectly regulate LysoPC (15:0/0:0), LysoPC (22:6 (4Z, 7Z, 10Z, 13Z, 16Z, 19Z)/0:0), LysoPC (18:3 (6Z, 9Z, 12Z)/0:0), LysoPC (20:2 (11Z, 14Z)/0:0), indoleacetaldehyde, sphinganine 1-phosphate and then affect glycerophospholipid metabolism, sphingolipid metabolism, tryptophan metabolism to play an anticancer effect.

3.9 Validation of critical targets

In order to investigate how GYP exerts its anti-LC effects by regulating metabolites and metabolic pathways as well as enhancing the anti-lung cancer effects of chemotherapeutic agents, the relative contents of STAT3, EGFR, MAPK14, and TYMS between the six groups were analyzed by western blot (Figure 11). MAPK14 and STAT3 play a carcinogenic role in the research mechanism of cancer cells (Yang et al., 2021). As shown in Figure 11, GYP group significantly inhibited the expression of STAT3, EGFR, TYMS and MAPK14 in tumor tissues compared with M group, the expression of STAT3, TYMS and MAPK14 in the GYP + cisplatin group ([PL] and [PH]) were significantly lower than that in the model group [M], single administration group ([P], [L] and [H] group). The findings suggested that GYP might exert anticancer effects in lung cancer and enhance the effects of chemotherapeutic agent cisplatin through the MAPK14/STAT3 signaling pathway.



recover 23 differential metabolites, and the effect of GYP on LLC mice might be related to six metabolic pathways, including alpha-Linolenic acid metabolism, glutathione metabolism, sphingolipid metabolism, glycerophospholipid metabolism, tryptophan metabolism, primary bile acid biosynthesis. Network analysis and metabolomics combined with western blot demonstrated that GYP might exert anti-lung cancer effects as well as enhance the pharmacological effects of the chemotherapeutic agent cisplatin through the MAPK14/STAT3 signaling pathway.

In our study, the relative contents of 3,5-tetradecadienoic acid, 12-hydroxydodecanoic acid and indole-3 acetaldehyde in the serum of mice in the model group decreased, while GYP

increased the levels of these metabolites; The relative contents of 12,13-DHOME, pseudouridine, sphinganine 1-phosphate and taurochenodesoxycholic acid in the serum of LLC mice in the model group was increased, but GYP decreased their levels. 3,5-tetradecadiencarnitine is one of the metabolic biomarkers of thyroid papillary carcinoma in different iodine nutrition regions, and it is related to iodine excess and cancer (Sun et al., 2021). Studies have shown that 12,13-DHOME comes from the oxidation of linoleic acid, which is related to an increased risk of ovarian cancer, cytochrome P450 monooxygenase oxidizes linoleic acid to produce 12,13-DHOME, the role of DHOME in multiple cellular functions may

lead to an increased risk of ovarian cancer (Hada et al., 2019). 12-Hydroxydodecanoic acid is one of the biomarkers of serum metabolites of colorectal cancer (Zhang et al., 2021). Indole-3 acetaldehyde is a precursor molecule for tryptophan to form endogenous 6-formylindolo [3,2-b] carbazole (ficz), tryptophan is related to tumor immune escape (Rannug, 2022). Pyridyl carnitine is one of the potential biomarkers for early diagnosis of hepatocellular carcinoma (HCC) (Kim et al., 2019). Pseudouridine was disturbed in patients with epithelial ovarian cancer (EOC), which might be a potential biomarker of EOC (Zhang et al., 2013). Sphinganine 1-phosphate (S1P) is one of the plasma biomarkers in patients with esophageal squamous cell carcinoma (ESCC), which can be used to diagnose ESCC, S1P could promote inflammation and mitosis, which may help to promote the progress of pancreatic cancer, S1P acts on specific G protein coupled receptors on immune, cardiovascular and nervous system cells, thereby regulating the induction of inflammation and cancer (Scherer et al., 2009). Taurochenodesoxycholic acid is a potential biomarker associated with liver cirrhosis (Yin et al., 2009).

GYP significantly reduced the expression of STAT3, EGFR, TYMS and MAPK14 in tumor tissues, while cisplatin combined with GYP could further reduce the expression of STAT3, TYMS and MAPK14 in tumor tissues. MAPK14 (also known as p38 MAPK) plays a crucial role in many processes, such as cell survival, differentiation (Liang et al., 2015). As a member of MAPK family, MAPK14 plays a vital role in the regulation of apoptosis, MAPK14 is also overexpressed in breast, ovary and cancer cells to promote tumorigenesis and development. STAT3 signal could promote the growth of non-small cell lung cancer (NSCLC) by promoting angiogenesis, cell survival, cancer cell stem cells, so STAT3 could affect tumorigenesis by controlling the survival, apoptosis and cell cycle of cancer cells, the activation of STAT3 can promote the secretion of proinflammatory cytokines, growth factors and chemokines (Parakh et al., 2021). The expression level of TYMS in colorectal cancer patients was significantly higher than that in normal control group (Jie et al., 2021). TYMS is a biomarker of pancreatic cancer, which is up-regulated in pancreatic cancer (Fu et al., 2019). Epidermal growth factor receptor (EGFR) is a carcinogen and activates various carcinogenic signaling pathways in cancer cells (Yang et al., 2022). Overexpression and activation of EGFR promote cell growth and metastasis of many cancers (Zhang et al., 2022). EGFR, as a receptor tyrosine kinase (RTK), is a carcinogen and a therapeutic target for many cancers, which can activate many carcinogenic signal pathways in cancer cells.

Studies have shown that tryptophan metabolism is significantly increased in tumors, which can promote tumorigenesis and immune escape (Cui et al., 2021). It is reported that there is a correlation between

glycerophospholipids metabolic disorder and tumorigenesis, and glycerophospholipids are associated with tumorigenesis and development, glycerophosphatides are the main components of biofilms (Chen et al., 2022), glycerolphospholipid metabolism is the most critical pathway associated with NSCLC (Wu et al., 2020). Lung cancer can cause regulation of sphingolipid metabolism, GYP can regulate this sphingolipid metabolism. Sphingolipids can effectively inhibit tumor formation (Lee et al., 2020). Sphingomyelin is a kind of sphingolipids, sphingolipids are key components of biofilms and participate in many processes related to tumor progression (Martin-Blazquez et al., 2019). However, there are still some deficiencies in this study, how GYP indirectly affect metabolites and metabolic pathways by affecting MAPK14/STAT3 signaling pathway still needs further research, we will carry out relevant research in the next step.

5 Conclusion

From the perspective of metabolomics and network pharmacology, we studied the mechanism of GYP on lung cancer and its mechanism of enhancing the anti-lung cancer pharmacological effects of cisplatin, GYP might exert anticancer effects as well as enhance the anticancer effects of cisplatin through the MAPK14/STAT3 signaling pathway, which provides a reference basis for the development of lung cancer drugs.

Data availability statement

The datasets presented in this study can be found in online repositories. The names of the repository/repositories and accession number(s) can be found in the article/Supplementary Material.

Ethics statement

The animal study was reviewed and approved by the Biological and Medical Ethics Committee of China University for Nationalities (ECMUC201903AO, 9 March 2019).

Author contributions

YQ performed, analyzed and wrote the manuscript. MX, PX, JX, MG, and FL prepared the GYP from *G. pentaphyllum*. XP designed research and revised the manuscript.

Funding

This work was supported financially by the National Natural Science Foundation of China (No. 82274209, 81673692); National Key R&D Program of China (No. 2017YFC1704000); The Doctoral Student's Independent Research Project of Minzu University of China (No. BBZZKY-2020041).

Conflict of interest

The authors declare that the research was conducted in the absence of any commercial or financial relationships that could be construed as a potential conflict of interest.

References

- Ahmad, B., Khan, S., Nabi, G., Gamallat, Y., Su, P., Jamal, Y., et al. (2019). Natural gypenosides: targeting cancer through different molecular pathways. *Cancer Manag. Res.* 11, 2287–2297. doi:10.2147/CMAR.S185232
- Cai, H., Wen, Z., Xu, X., Wang, J., Li, X., Meng, K., et al. (2022). Serum metabolomics analysis for biomarkers of lactobacillus plantarum FRT4 in high-fat diet-induced obese mice. *Foods* 11, 184. doi:10.3390/foods11020184
- Chen, M. H., Zhou, J., Wu, C. Y., Zhang, W., Long, F., Zhou, S. S., et al. (2022). Gut microbiota influenced the xenograft MC38 tumor growth potentially through interfering host lipid and amino acid metabolisms, basing on the integrated analysis of microbiome and metabolomics. *J. Chromatogr. B Anal. Technol. Biomed. Life Sci.* 1192, 123136. doi:10.1016/j.jchromb.2022.123136
- Cheung, P. K., Ma, M. H., Tse, H. F., Yeung, K. F., Tsang, H. F., Chu, M. K. M., et al. (2019). The applications of metabolomics in the molecular diagnostics of cancer. *Expert Rev. Mol. Diagn.* 19, 785–793. doi:10.1080/14737159.2019.1656530
- Cui, M., Liu, D., Xiong, W., Wang, Y., and Mi, J. (2021). ERRFI1 induces apoptosis of hepatocellular carcinoma cells in response to tryptophan deficiency. *Cell Death Discov.* 7, 274. doi:10.1038/s41420-021-00666-y
- Fu, Z., Jiao, Y., Li, Y., Ji, B., Jia, B., and Liu, B. (2019). TYMS presents a novel biomarker for diagnosis and prognosis in patients with pancreatic cancer. *Med. Baltim.* 98, e18487. doi:10.1097/MD.00000000000018487
- Hada, M., Edin, M. L., Hartge, P., Lih, F. B., Wentzensen, N., Zeldin, D. C., et al. (2019). Prediagnostic serum levels of fatty acid metabolites and risk of ovarian cancer in the prostate, lung, colorectal, and ovarian (PLCO) cancer screening trial. *Cancer Epidemiol. Biomarkers Prev.* 28, 189–197. doi:10.1158/1055-9965.EPI-18-0392
- Jie, Y., Yang, X., and Chen, W. (2021). Expression and gene regulation network of TYMS and BCL2L1 in colorectal cancer based on data mining. *PeerJ* 9, e11368. doi:10.7717/peerj.11368
- Kim, D. J., Cho, E. J., Yu, K. S., Jang, I. J., Yoon, J. H., Park, T., et al. (2019). Comprehensive metabolomic search for biomarkers to differentiate early stage hepatocellular carcinoma from cirrhosis. *Cancers (Basel)* 11, E1497. doi:10.3390/cancers11101497
- Kim, Y. H., Jung, J. I., Jeon, Y. E., Kim, S. M., Hong, S. H., Kim, T. Y., et al. (2022a). Gynostemma pentaphyllum extract and its active component gypenoside L improve the exercise performance of treadmill-trained mice. *Nutr. Res. Pract.* 16, 298–313. doi:10.4162/nrp.2022.16.3.298
- Kim, Y. H., Jung, J. I., Jeon, Y. E., Kim, S. M., Oh, T. K., Lee, J., et al. (2022b). Gynostemma pentaphyllum extract and Gypenoside L enhance skeletal muscle differentiation and mitochondrial metabolism by activating the PGC-1 α pathway in C2C12 myotubes. *Nutr. Res. Pract.* 16, 14–32. doi:10.4162/nrp.2022.16.1.14
- Lee, Y. R., An, K. Y., Jeon, J., Kim, N. K., Lee, J. W., Hong, J., et al. (2020). Untargeted metabolomics and polyamine profiling in serum before and after surgery in colorectal cancer patients. *Metabolites* 10, E487. doi:10.3390/metabo10120487
- Li, W., Ma, G., Deng, Y., Wu, Q., Wang, Z., and Zhou, Q. (2021). Artesunate exhibits synergistic anti-cancer effects with cisplatin on lung cancer A549 cells by inhibiting MAPK pathway. *Gene* 766, 145134. doi:10.1016/j.gene.2020.145134
- Li, X., Liu, H., Lv, C., Du, J., Lian, F., Zhang, S., et al. (2022). Gypenoside-Induced apoptosis via the PI3K/AKT/mTOR signaling pathway in bladder cancer. *Biomed. Res. Int.* 2022, 9304552. doi:10.1155/2022/9304552
- Liang, N., Zhong, R., Hou, X., Zhao, G., Ma, S., Cheng, G., et al. (2015). Ataxia-telangiectasia mutated (ATM) participates in the regulation of ionizing radiation-induced cell death via MAPK14 in lung cancer H1299 cells. *Cell Prolif.* 48, 561–572. doi:10.1111/cpr.12203
- Liang, Q. C., and Zhong, M. (2005). *Chinese Zhuang medicine*. China: Guangxi nationalities publishing house.
- Liu, H., Li, X., Duan, Y., Xie, J. B., and Piao, X. L. (2021). Mechanism of gypenosides of Gynostemma pentaphyllum inducing apoptosis of renal cell carcinoma by PI3K/AKT/mTOR pathway. *J. Ethnopharmacol.* 271, 113907. doi:10.1016/j.jep.2021.113907
- Martin-Blazquez, A., Diaz, C., Gonzalez-Flores, E., Franco-Rivas, D., Jimenez-Luna, C., Melguizo, C., et al. (2019). Untargeted LC-HRMS-based metabolomics to identify novel biomarkers of metastatic colorectal cancer. *Sci. Rep.* 9, 20198. doi:10.1038/s41598-019-55952-8
- Noreldeen, H. A. A., Liu, X., and Xu, G. (2020). Metabolomics of lung cancer: Analytical platforms and their applications. *J. Sep. Sci.* 43, 120–133. doi:10.1002/jssc.201900736
- Parakh, S., Ernst, M., and Poh, A. R. (2021). Multicellular effects of STAT3 in non-small cell lung cancer: Mechanistic insights and therapeutic opportunities. *Cancers (Basel)* 13, 6228. doi:10.3390/cancers13246228
- Qi, Y. S., Xie, J. B., Xie, P., Duan, Y., Ling, Y. Q., Gu, Y. L., et al. (2021). Uncovering the anti-NSCLC effects and mechanisms of gypenosides by metabolomics and network pharmacology analysis. *J. Ethnopharmacol.* 281, 114506. doi:10.1016/j.jep.2021.114506
- Qiu, W. L., Hsu, W. H., Tsao, S. M., Tseng, A. J., Lin, Z. H., Hua, W. J., et al. (2021). WSG, a glucose-rich polysaccharide from ganoderma lucidum, combined with cisplatin potentiates inhibition of lung cancer *in vitro* and *in vivo*. *Polym. (Basel)* 13, 4353. doi:10.3390/polym13244353
- Rannug, A. (2022). 6-Formylindolo[3, 2-b]carbazole, a potent ligand for the aryl hydrocarbon receptor produced both endogenously and by microorganisms, can either promote or restrain inflammatory responses. *Front. Toxicol.* 4, 775010. doi:10.3389/ftox.2022.775010
- Scherer, M., Schmitz, G., and Liebisch, G. (2009). High-throughput analysis of sphingosine 1-phosphate, sphinganine 1-phosphate, and lysophosphatidic acid in plasma samples by liquid chromatography-tandem mass spectrometry. *Clin. Chem.* 55, 1218–1222. doi:10.1373/clinchem.2008.113779
- Schmidt, D. R., Patel, R., Kirsch, D. G., Lewis, C. A., Vander Heiden, M. G., and Locasale, J. W. (2021). Metabolomics in cancer research and emerging applications in clinical oncology. *Ca. Cancer J. Clin.* 71, 333–358. doi:10.3322/caac.21670
- Sun, Q., Zhao, H., Liu, Z., Wang, F., He, Q., Xiu, C., et al. (2021). Identifying potential metabolic tissue biomarkers for papillary thyroid cancer in different iodine nutrient regions. *Endocrine* 74, 582–591. doi:10.1007/s12020-021-02773-3
- Tayanloo-Beik, A., Sarvari, M., Payab, M., Gilany, K., Alavi-Moghadam, S., Gholami, M., et al. (2020). OMICS insights into cancer histology; Metabolomics and proteomics approach. *Clin. Biochem.* 84, 13–20. doi:10.1016/j.clinbiochem.2020.06.008
- Wu, H., Chen, Y., Li, Q., Gao, Y., Zhang, X., Tong, J., et al. (2018). Intervention effect of Qi-Yu-San-Long Decoction on Lewis lung

Publisher's note

All claims expressed in this article are solely those of the authors and do not necessarily represent those of their affiliated organizations, or those of the publisher, the editors and the reviewers. Any product that may be evaluated in this article, or claim that may be made by its manufacturer, is not guaranteed or endorsed by the publisher.

Supplementary material

The Supplementary Material for this article can be found online at: <https://www.frontiersin.org/articles/10.3389/fphar.2022.1070948/full#supplementary-material>

carcinoma in C57BL/6 mice: Insights from UPLC-QTOF/MS-based metabolic profiling. *J. Chromatogr. B Anal. Technol. Biomed. Life Sci.* 1102–1103, 23–33. doi:10.1016/j.jchromb.2018.10.013

Wu, H., Wang, L., Zhan, X., Wang, B., Wu, J., and Zhou, A. (2020). A UPLC-Q-TOF/MS-based plasma metabolomics approach reveals the mechanism of Compound Kushen Injection-based intervention against non-small cell lung cancer in Lewis tumor-bearing mice. *Phytomedicine* 76, 153259. doi:10.1016/j.phymed.2020.153259

Yang, L., Bhattacharya, A., Li, Y., Sexton, S., Ling, X., Li, F., et al. (2022). Depleting receptor tyrosine kinases EGFR and HER2 overcomes resistance to EGFR inhibitors in colorectal cancer. *J. Exp. Clin. Cancer Res.* 41, 184. doi:10.1186/s13046-022-02389-z

Yang, L., Wang, Y., Cai, H., Wang, S., Shen, Y., and Ke, C. (2020). Application of metabolomics in the diagnosis of breast cancer: a systematic review. *J. Cancer* 11, 2540–2551. doi:10.7150/jca.37604

Yang, W., Su, J., Li, M., Li, T., Wang, X., Zhao, M., et al. (2021). Myricetin induces autophagy and cell cycle arrest of HCC by inhibiting MARCH1-regulated Stat3 and p38 MAPK signaling pathways. *Front. Pharmacol.* 12, 709526. doi:10.3389/fphar.2021.709526

Yao, L., Cheng, S., Yang, J., Xiang, F., Zhou, Z., Zhang, Q., et al. (2022). Metabolomics reveals the intervention effect of Zhuang medicine

Longzuantongbi granules on a collagen-induced arthritis rat model by using UPLC-MS/MS. *J. Ethnopharmacol.* 294, 115325. doi:10.1016/j.jep.2022.115325

Yin, P., Wan, D., Zhao, C., Chen, J., Zhao, X., Wang, W., et al. (2009). A metabolomic study of hepatitis B-induced liver cirrhosis and hepatocellular carcinoma by using RP-LC and HILIC coupled with mass spectrometry. *Mol. Biosyst.* 5, 868–876. doi:10.1039/b820224a

Zhang, C., Zhou, S., Chang, H., Zhuang, F., Shi, Y., Chang, L., et al. (2021). Metabolomic profiling identified serum metabolite biomarkers and related metabolic pathways of colorectal cancer. *Dis. Markers* 2021, 6858809. doi:10.1155/2021/6858809

Zhang, J. J., Cao, C. X., Wan, L. L., Zhang, W., Liu, Z. J., Wang, J. L., et al. (2022). Forkhead Box q1 promotes invasion and metastasis in colorectal cancer by activating the epidermal growth factor receptor pathway. *World J. Gastroenterol.* 28, 1781–1797. doi:10.3748/wjg.v28.i17.1781

Zhang, T., Wu, X., Ke, C., Yin, M., Li, Z., Fan, L., et al. (2013). Identification of potential biomarkers for ovarian cancer by urinary metabolomic profiling. *J. Proteome Res.* 12, 505–512. doi:10.1021/pr3009572

Zhao, G. P., Dai, S., and Chen, R. S. (2006). *Dictionary of traditional Chinese medicine*. Edition 2. China: Shanghai Scientific & Technical Publishers.